ACS Chemical Neuroscience

pubs.acs.org/chemneuro Research Article

Evaluation of [^{18}F]-*N*-Methyl-lansoprazole as a Tau PET Imaging Agent in First-in-Human Studies

Vasko Kramer,*,▽ Allen F. Brooks,*,▽ Arlette Haeger, Rodrigo Kuljis, Waqas Rafique, Robert A. Koeppe, David M. Raffel, Kirk A. Frey, Horacio Amaral, Peter J. H. Scott,* and Patrick J. Riss*

Cite This: https://dx.doi.org/10.1021/acschemneuro.9b00639 Read Online

ACCESS | Metrics & More | Article Recommendations | Supporting Information

ABSTRACT: Development of positron emission tomography (PET) imaging agents capable of quantifying tau aggregates in neurodegenerative disorders such as Alzheimer's disease (AD) is of enormous importance in the field of dementia research. The aim of the present study was to conduct first-in-man imaging studies with the potential novel tau imaging agent [^{18}F]-*N*-methyl lansoprazole ([^{18}F]NML). Herein we report validation of the synthesis of [^{18}F]NML for clinical use by labeling the trifluoromethyl group via radiofluorination of the corresponding *gem*-difluoro enol ether precursor. This is the first use of this method for clinical production of PET radiotracers and confirmed that it can be readily implemented at multiple production facilities to provide [^{18}F]NML in good noncorrected radiochemical yield (3.4 ± 1.5 GBq, 4.6% ± 2.6%) and molar activity (120.1 ± 186.3 GBq/μmol), excellent radiochemical purity (>97%), and suitable for human use (n = 15). With [^{18}F]NML in hand, we conducted rodent biodistribution, estimates of human dosimetry, and preliminary evaluation of [^{18}F]NML in human subjects at two imaging sites. Healthy controls (n = 4) and mildly cognitively impaired (MCI) AD patients (n = 6) received [^{18}F]NML (tau), [^{18}F]AV1451 (tau), and [^{18}F]florbetaben or [^{18}F]florbetapir (amyloid) PET scans. A single progressive supranuclear palsy (PSP) patient also received [^{18}F]NML and [^{18}F]AV1451 PET scans. [^{18}F]NML showed good brain uptake, reasonable pharmacokinetics, and appropriate imaging characteristics in healthy controls. The mean ± SD of the administered mass of [^{18}F/^{19}F]NML was 2.01 ± 2.17 μg (range, 0.16−8.27 μg) and the mean administered activity was 350 ± 62 MBq (range, 199−403 MBq). There were no adverse or clinically detectable pharmacologic effects in any of the 11 subjects, and no significant changes in vital signs were observed. However, despite high affinity for tau *in vitro*, brain retention in MCI/AD and PSP patients was low, and there was no evidence of specific signals *in vivo* that corresponded to tau. Although it is still unclear why clinical translation of the radiotracer was unsuccessful, we nevertheless conclude that further development of [^{18}F]NML as a tau PET imaging agent is not warranted at this time.

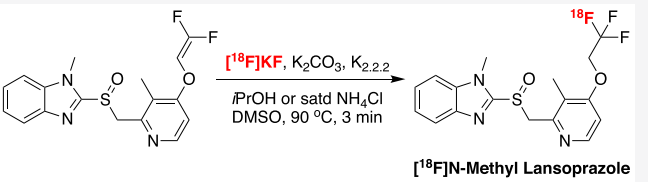

KEYWORDS: *[^{18}F]N-Methyl-Lansoprazole, Neurofibrillary tangles, Alzheimer's Disease, tau imaging*

INTRODUCTION

Aggregated tau protein (with either 3 repeat units (3R) or 4 repeat units (4R)) is a hallmark pathology of neurodegenerative disorders such as Alzheimer's disease (AD) and related tauopathies that correlates with cognitive decline and Braak staging.[1] Reflecting this, there is significant interest in developing imaging agents for quantifying tau aggregates using positron emission tomography (PET) imaging (for recent reviews of tau PET, see refs 2−9). Despite significant progress to date, there remain challenges with tau imaging. For example, first generation tau tracers such as [^{18}F]THK5351[10] and [^{18}F]AV1451[11] suffer from off-target binding to monoamine oxidase,[12−14] while [^{11}C]PBB3 is associated with brain-penetrating metabolites.[15] As such, development continues and a number of new second generation tau imaging agents have been reported recently and are all currently in clinical trials, including [^{18}F]MK6240,[16,17] [^{18}F]PI-2620,[18] [^{18}F]-GTP1,[19] [^{18}F]RO6958948,[20] and fluorinated PBB3 derivatives.[21]

Imaging of 3R tau looks promising for these new second generation agents. However, while [^{18}F]PI-2620 appears to bind to all subtypes of tau (3R, 4R, 3R/4R),[22] there is still no imaging agent that is selective for 4R tau found in tauopathies such as progressive supranuclear palsy (PSP) and corticobasal degeneration (CBD).[23] With these various issues in mind, we have investigated development of tau PET imaging agents based upon the proton pump inhibitor lansoprazole, after it was shown to have high affinity for tau aggregates *in vitro* (K_i = 2.5 nM for heparin-induced tau filaments).[24] With the aim of repurposing the lansoprazole scaffold for tau PET, we recently reported the radiosynthesis and preclinical evaluation of lansoprazole derivatives, including [^{18}F]*N*-methyl lansoprazole

Received: November 27, 2019
Accepted: January 3, 2020
Published: January 3, 2020

([^{18}F]NML), as potential tau imaging agents.[25−27] These studies demonstrated that [^{18}F]NML has high affinity for heparin-induced tau filaments (K_d = 0.7 nM) and 11.7-fold selectivity for tau over amyloid. This selectivity could perhaps be better, but an order of magnitude is in line with the 20-fold selectivity that has been suggested as a target for the ideal tau radiotracer.[9] Autoradiography and binding affinity studies confirmed that [^{18}F]NML binds to both the 3R/4R tau found in AD (K_d = 8.2 nM[25]) and 4R tau found in PSP (K_d = 11.4 nM[28]). *In vivo* preclinical imaging studies in healthy rodents and non-human primates also revealed high brain uptake, as well as favorable imaging properties and brain pharmacokinetics.[25] Given these promising results, we were motivated to evaluate [^{18}F]NML in a clinical setting. In this paper, we report validation of the synthesis of [^{18}F]NML for clinical use from its respective *gem*-difluoro enol ether precursor, through radiofluorination of the trifluoromethyl group. With [^{18}F]NML in hand, we conducted rodent biodistribution studies, estimates of human dosimetry, and, to our knowledge, the first-in-human PET study with [^{18}F]NML comparing healthy control subjects to dementia patients. Healthy controls (n = 4) and mildly cognitively impaired (MCI) AD patients (n = 6) received [^{18}F]NML (tau), [^{18}F]AV1451 (tau), and [^{18}F]florbetaben or [^{18}F]florbetapir (amyloid) PET scans at PositronMed (PM, Chile) and the University of Michigan (UM, USA). An additional PSP patient also received [^{18}F]NML and [^{18}F]-AV1451 PET scans at UM.

RESULTS AND DISCUSSION

Validation of the Radiosynthesis of [^{18}F]NML. [^{18}F]NML is synthesized from the *gem*-difluoro enol ether precursor **1** using no-carrier-added [^{18}F]KF in the presence of [2.2.2]cryptand (kryptofix 222, crypt-222) and a proton source (*i*PrOH or NH_4Cl) to quench the reaction and allow generation of the trifluormethyl group, as previously reported (Scheme 1).[25,27,29] These prior syntheses provided [^{18}F]NML

Scheme 1. Radiosynthesis of [^{18}F]NML

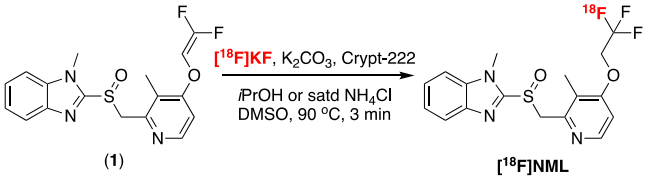

suitable for preclinical use but, in order to prepare [^{18}F]NML for clinical use, a radiosynthesis compliant with current Good Manufacturing Practice (cGMP) needed to be validated. During our initial studies, we found that formation of high molar activity [^{18}F]trifluoromethyl groups can be challenging because of isotopic exchange as well as fluoride ion release through precursor degradation.[25,29,30] Following careful balancing of radiochemical yield, reaction time, and temperature (see Supporting Information for details of optimization experiments), qualification runs were performed using the established production method (see Methods section for full details), and we were gratified to observe that [^{18}F]NML was formed in good molar activity during these validation runs (molar activity at University of Michigan = 36.6 ± 14.8 GBq/μmol; molar activity at PositronMed = 226.6 ± 310.9 GBq/μmol). The apparent difference in molar activity between sites is down to one outlier (see Supporting Information). Doses of [^{18}F]NML also met or exceeded all quality control criteria, confirming suitability for clinical use (Table 1).

Rodent Biodistribution and Estimated Human Dosimetry. Biodistribution studies were conducted in male and female Sprague−Dawley rats to determine radiation-absorbed-dose estimates using the OLINDA/EXM 1.0 software package.[31] In the study, [^{18}F]NML was administered iv via the tail vein, and animals were sacrificed and sectioned at four time points: 5, 30, 60, and 120 min. The data for the biodistribution (see Table S1 and Figure S2 in Supporting Information) showed rapid distribution throughout the body, with highest uptake observed in contents of the stomach and small intestine and is consistent with that previously reported for [^{11}C]NML.[26] The biodistribution studies also confirmed brain uptake of the radiotracer. In addition, small animal PET scans of 4 rats (2 male and 2 female) were taken with the bladder in frame, to determine distribution in the urine. This data was then used to calculate radiation-absorbed-dose estimates for humans to facilitate first-in-human studies (Table 2 and Table S2 in Supporting Information).

Imaging in Healthy Controls and Patients with MCI/AD or PSP. Clinical PET studies were conducted at two sites: PositronMed (Chile) and the University of Michigan (USA) (Table 3). A total of five participants were included in the prospective study at the site in Chile, including two healthy volunteers (mean ± SD age 57.5 ± 7.8 years) to study physiological distribution of [^{18}F]NML in the brain and three patients (mean ± SD age 72.0 ± 6.0 years), clinically diagnosed with mild to moderate AD, to study tracer binding to neurofibrillary tangles consisting of pathologic tau aggregates. All subjects participated at least in the [^{18}F]NML PET/CT scan. One HC and two AD patients also participated in a volumetric 3D 1.5 T MRI scan for co-registration, whereas one HC (HC-1) and one AD (AD-3) patient were not able to participate in the MRI scan. In addition, two AD patients (AD-1 and AD-2) had a positive β-amyloid PET/CT scan with [^{18}F]florbetaben ([^{18}F]FBB) and participated in an additional PET/CT scan with [^{18}F]AV1451 to confirm presence of neurofibrillary tangles (see Table 3).

At the site in Michigan, an additional six participants were included in the study (Table 3). Two healthy volunteers (mean age 65 ± 4 years) were included to also investigate physiological distribution of [^{18}F]NML in the brain. Three patients (mean age 77 ± 9 years) clinically diagnosed with mild to moderate AD (official clinical diagnosis of MCI (amnestic)) and one patient (age 76 years) clinically diagnosed with PSP were included to study tracer binding to 3R and 4R tau. Structural brain MR imaging was performed before [^{18}F]NML PET. [^{18}F]NML (384−403 MBq) was administered by intravenous bolus. All subjects received additional [^{18}F]AV1451 scans, and AD patients also received [^{18}F]florbetapir scans.

[^{18}F]NML administration was well tolerated by all subjects at both study sites. Administered mass dosages of NML were 2.01 ± 2.17 μg (n = 11; range, 0.16−8.27 μg). No alterations were noted in vital signs or in physical or neurological examinations, nor were significant changes noted in either electrocardiograms or any of the laboratory values.

From imaging results in healthy subjects as well as MCI/AD (Figures 1−3) and PSP (Figure 4) patients, [^{18}F]NML showed good penetration into brain tissue with a peak uptake of 5.0−6.0% of the injected dose (i.D.) during the initial perfusion phase, 1 min postinjection (p.i.), and fast clearance from brain

https://dx.doi.org/10.1021/acschemneuro.9b00639
ACS Chem. Neurosci. XXXX, XXX, XXX−XXX

Table 1. QC Data for [^{18}F]NML Validation Runs

QC test	specifications	Michigan (n = 4)	Positronpharma (n = 5)
radioactivity concn	≥370 MBq/batch	2.8 ± 0.7 GBq	2.4 ± 1.8 GBq
NML concn	[a]	3.3 ± 2. Seven μg/mL	0.9 ± 0.8 μg/mL
molar activity	≥14.1 GBq/μmol[b]	37 ± 15 GBq/μmol	233 ± 324 GBq/μmol
mass limit	≤10 μg/injection	2.80 ± 2.73 μg	1.06 ± 0.61 μg
radiochemical purity	>95%	100% ± 0%	97.7% ± 0.8%
identity	RRT[c] = 0.9−1.1	1.0 ± 0.0	1.0 ± 0.0
visual inspection	clear, colorless, no ppt	pass	pass
pH	4.5−7.5	5.0 ± 0.0	5.0 ± 0.0
radionuclidic identity	$t_{1/2}$ = 105−115 min	109 ± 2 min	110 ± 2 min
residual crypt-222	≤50 μg/mL	<50 μg/mL	<50 μg/mL
residual DMSO	≤5000 ppm	19 ± 13 ppm	11.4 ± 16.7 ppm
residual MeCN	≤410 ppm	24 ± 3 ppm	0.92 ± 1.41 ppm
filter membrane integrity	≥44 psi	49 ± 2 psi	>50 psi
bacterial endotoxins	≤2.00 EU[d]/mL	<2.00 EU[b]/mL	<1.75 EU[d]/mL
sterility	no microbial growth	pass	pass

[a]Not applicable. [b]Based on worst case scenario of 10 μg in a 370 MBq injection. [c]Relative retention time (RRT) = [(HPLC retention time of [^{18}F]NML)/(HPLC retention time of NML reference standard)]. [d]EU = endotoxin units.

Table 2. Radiation-Absorbed-Dose Estimates for Humans Calculated Using OLINDA/EXM 1.0 with Preclinical Rodent Studies[a]

target organ	total dose (mSv/MBq)	dose for 370 MBq injection (mSv)
adrenals	0.011	3.96
brain	0.004	1.60
breasts	0.008	3.12
gallbladder wall	0.017	6.18
lower lower intestine wall	0.031	11.40
upper lower intestine wall	0.070	25.90
small intestine	0.064	23.50
stomach wall	0.015	5.44
heart wall	0.009	3.17
kidneys	0.012	4.29
liver	0.011	4.22
lungs	0.007	2.76
muscle	0.011	4.14
ovaries	0.021	7.88
pancreas	0.011	4.00
red marrow	0.011	4.18
osteogenic cells	0.016	6.03
skin	0.008	3.08
spleen	0.012	4.40
testes	0.011	4.11
thymus	0.010	3.81
thyroid	0.010	3.85
urinary bladder wall	0.052	19.20
uterus	0.021	7.59
total body	0.012	4.40
effective dose	0.019	6.85

[a]See Supporting Information for full details.

tissue. We observed retention of the tracer in white matter regions, which might be related to binding of the tracer to β-sheet-rich myelinated tissue as observed for other tracers.[32] Binding could be observed within 10−30 min p.i., followed by rapid and complete clearance until the end of the scan.

Tracer uptake in healthy controls at later time points was low (SUV_{bw} = 0.50−0.75 at 60−90 min p.i.), distribution was homogeneous throughout the whole brain, and no difference could be observed between regions-of-interest and cerebellar gray matter as reference region. Surprisingly the same homogeneous distribution pattern could be observed for [^{18}F]NML in all MCI/AD (Figures 1 and 2) and PSP (Figure 4) patients, and no specific uptake was observed during any time point of the scans. The same could be observed when looking at the tracer kinetics for different brain regions. For example, in the AD patients, time−activity curves for cortical gray matter (frontal, parietal, occipital, and temporal lobe) follow the same kinetic profile as the reference region (Figure 1). The only difference noted between healthy subjects and AD patients was a larger variation in blood flow and perfusion during the initial phase of the scan noted by a larger spread of the curves, which might be related to advanced atrophy in different regions as seen for the AD subject in Figure 1.

In order to confirm the presence of amyloid as well as neurofibrillary tangles and paired helical tau filaments (PHF-tau) in the MCI/AD patients, five patients received β-amyloid scans (with [^{18}F]florbetaben or [^{18}F]florbetapir) and an additional tau PET scan with [^{18}F]AV1451. The additional scans in these five MCI/AD patients confirmed the presence of both β-amyloid and PHF-tau. For example, subjects AD-1 and AD-2 showed significant tracer uptake with [^{18}F]AV1451 in every cortical brain region, with the temporal lobe being the most affected and frontal lobe being the least affected region in both patients (Figure 2). Typical off-target binding of [^{18}F]AV1451 in the basal ganglia and choroid plexus was also apparent in the scans as expected.[13] The distribution pattern of amyloid and tau deposits is different in each case, with [^{18}F]florbetaben or [^{18}F]florbetapir showing highest uptake in frontal cortex, consistent with cortical amyloid deposition.[33] For every MCI/AD patient scanned, no specific uptake could be observed for [^{18}F]NML in any brain region, which implies that [^{18}F]NML does not bind to PHF-tau or β-amyloid plaques *in vivo*. This is in contrast to previous findings from *in vitro* studies with post-mortem AD brain tissue and heparin-induced tau filaments conducted by three independent groups around the world, including our laboratories.[24−27]

To quantify and compare tracer uptake of [^{18}F]NML and [^{18}F]AV1451, as well as the PHF-tau burden in AD patients, we calculated SUV-ratios (SUVR) between regions of interest

https://dx.doi.org/10.1021/acschemneuro.9b00639
ACS Chem. Neurosci. XXXX, XXX, XXX−XXX

Table 3. Study Population and Clinical Data

subject	site	gender	age, years	body weight, kg	condition	β-amyloid PET	tau PET	[^{18}F]NML PET[b]	dose, MBq	injected mass, μg
HC-1	PM	F	52	47	HC	*a*	*a*	4/15/16	339	0.16
HC-2	PM	F	63	70	HC	*a*	*a*	4/21/16	308	1.61
HC-3	UM	F	67	68	HC	*a*	*a*	7/3/18	384	1.87
HC-4	UM	M	62	90	HC	*a*	*a*	7/11/18	386	1.38
AD-1	PM	F	72	52	AD	+	+	4/19/16	316	1.25
AD-2	PM	F	78	61	AD	+	+	5/12/16	199	0.76
AD-3	PM	F	66	65	AD	*a*	*a*	5/13/16	323	1.54
AD-4	UM	M	84	99	MCI	*a*	+	10/18/18	399	1.05
AD-5	UM	F	66	73	MCI	*a*	+	11/2/18	399	2.67
AD-6	UM	F	80	48	MCI	*a*	+	11/12/18	400	1.58
PSP-1	UM	M	76	76	PSP	*a*	+	9/19/19	403	8.27

[a]Not applicable. [b]Date of scan presented as month/day/year.

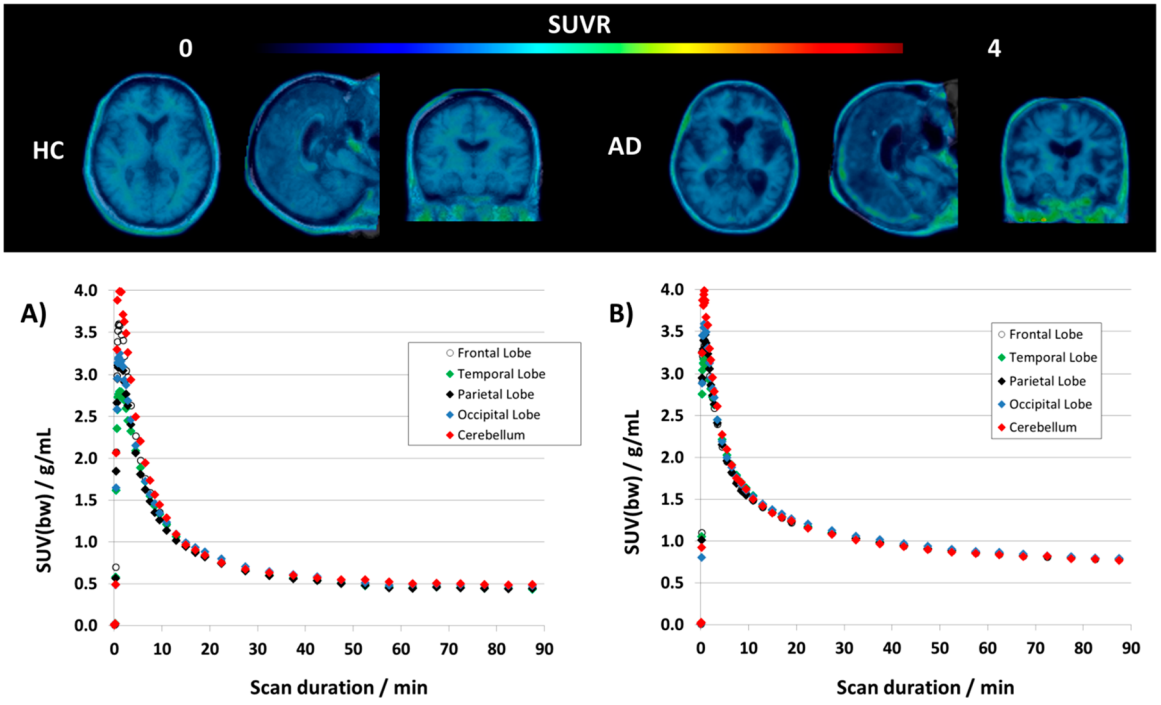

Figure 1. (top) Transversal, sagittal, and coronal view of averaged PET/MRI fusion images of [^{18}F]NML uptake in a healthy control (left) and an AD patient (right) 60−90 min postinjection. (bottom) TACs for [^{18}F]NML for cortical gray matter regions (frontal, parietal, temporal, and occipital lobe, as well as for cerebellum as reference region) of a healthy volunteer (A) and an AD patient (B).

and cerebellar gray matter as reference region for AD-1 and AD-2 (Figure 3). AD subjects showed SUVR values for [^{18}F]AV1451 of >2.0 for almost all brain regions and peak SUVR of 2.99 and 3.14 in medial temporal gyrus for subject AD-1 and AD-2, respectively. As reference, the $SUVR_{80-100}$ value provides reasonable outcome measures for differentiation between older normal controls (ONCs), MCI, and AD patients.[34] Average SUVR in medial temporal gyrus in those cohorts were 1.09 ± 0.14, 1.38 ± 0.18, and 1.78 ± 0.48 for ONC, MCI, and AD, respectively. As expected from the qualitative imaging results, SUV values for [^{18}F]NML were not significantly different from the reference region, with slightly lower values probably due to reduced perfusion.

Last, since [^{18}F]NML was found to also have high affinity for 4R tau *in vitro*,[26,25,28] we were curious whether the radiotracer could be used for tau imaging in 4R tauopathies such as progressive supranuclear palsy (PSP). Therefore, we also scanned one PSP patient with [^{18}F]NML in this study. Unfortunately, the same homogeneous distribution of [^{18}F]NML was observed in the PSP patient as was seen in the MCI/AD patients, and no obvious specific uptake was observed during any time point of the scan (Figure 4). The PSP patient was also scanned with [^{18}F]AV1451 the following week. That scan showed presumed off-target binding in the substantia nigra and choroid plexus but also possible tau signal in the globus pallidum and the lateral temporal lobe consistent with previous [^{18}F]AV1451 data in PSP subjects.[35,36] While post-mortem confirmation of tau is needed, this signal was not apparent in the [^{18}F]NML image.

This study demonstrates the complexity of developing a new PET imaging agent and that radiotracers that appear promising in preclinical evaluation can still fail in the clinic. While [^{18}F]NML showed good brain uptake in both non-human primates and human subjects, as well as high affinity for both 3R and 4R tau *in vitro*, this did not translate to successful imaging of tau in either MCI/AD or PSP patients. It is unclear at this point why [^{18}F]NML failed to image tau in these first clinical studies. However, perhaps known discrepancies

https://dx.doi.org/10.1021/acschemneuro.9b00639
ACS Chem. Neurosci. XXXX, XXX, XXX−XXX

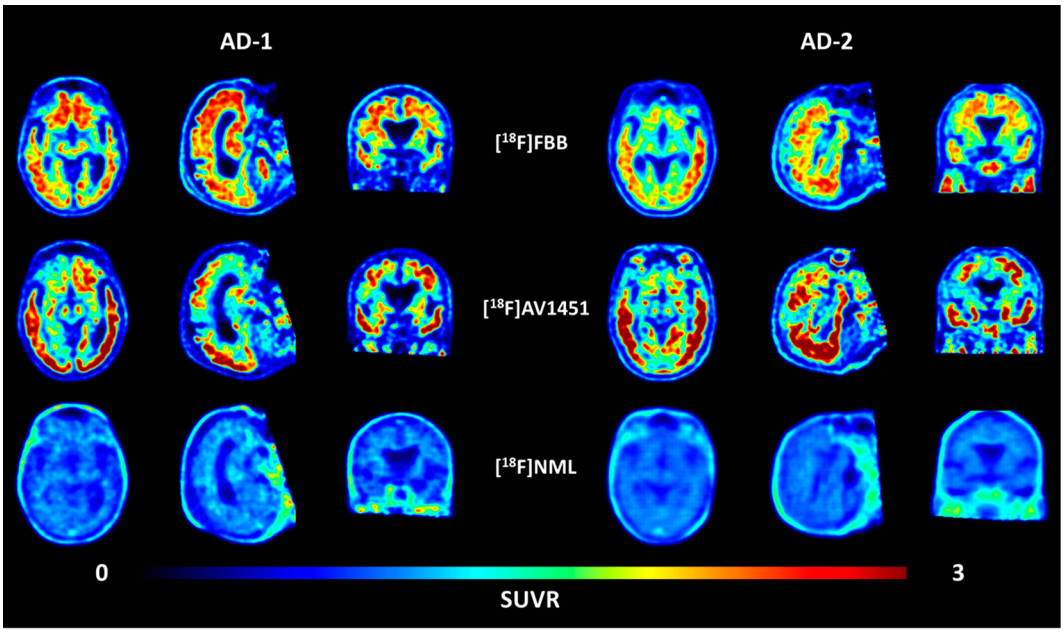

Figure 2. Transversal, sagittal, and coronal view of averaged PET images of [^{18}F]florbetaben (upper row), [^{18}F]AV1451 (middle row), and [^{18}F]NML (lower row) uptake in two AD patients 90−110, 80−100, and 60−90 min p.i., respectively.

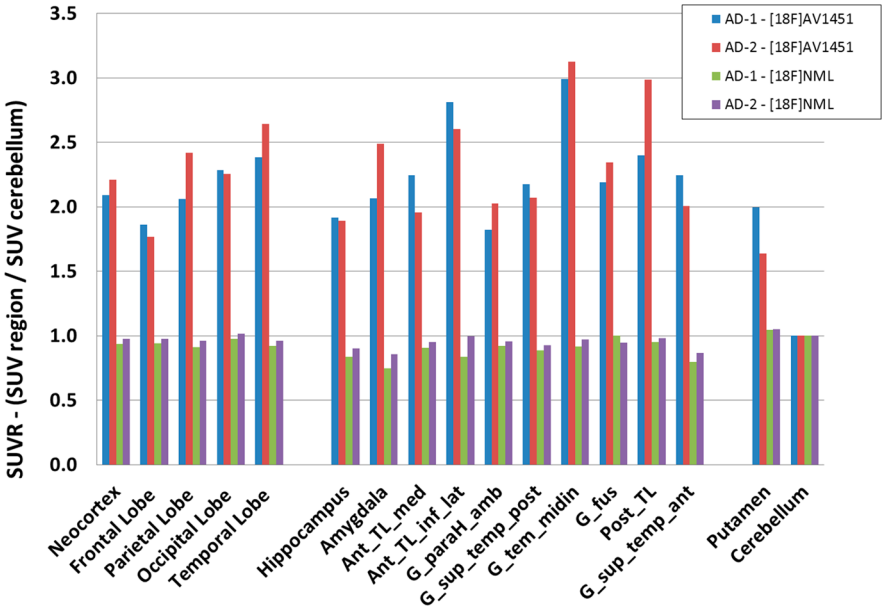

Figure 3. SUVR values of [^{18}F]NML (green and violet) and [^{18}F]AV1451 (blue and red) from two AD patients for frontal cortex, parietal cortex, temporal cortex, occipital cortex, neocortex, putamen, hippocampus, and different subregions of temporal cortex using cerebellar cortex as reference region.

between *in vitro* and *in vivo* results stemming from some combination of (i) tracer metabolism issues (while a favorable metabolism profile of [^{11}C]NML in rodent has been reported previously,[26] a limitation of the present study is that [^{18}F]NML metabolism was not determined in the clinical studies; in a preliminary study in one healthy subject, two venous blood samples were taken (10 and 20 min p.i.) and, after removal of blood cells and proteins, HPLC analysis revealed only parent [^{18}F]NML; however, more extensive metabolite analysis at later time points was not conducted), (ii) potential differences in disease stage between living patients and end-stage post-mortem samples, and (iii) inherent limitations of auto-radiography experiments[23] mean that the binding potential (BP) for [^{18}F]NML is simply insufficient to detect tau pathology *in vivo*.

CONCLUSIONS

In this study, we have successfully synthesized [^{18}F]NML in good molar activity by labeling its trifluoromethyl group and translated the radiotracer into first-in-human studies to investigate its use as a tau PET imaging agent. [^{18}F]NML was safe and well tolerated by all study participants. The tracer showed good brain uptake, reasonable pharmacokinetics, and appropriate imaging characteristics in healthy controls. However, despite high affinity for 3R and 4R tau *in vitro*,

https://dx.doi.org/10.1021/acschemneuro.9b00639
ACS Chem. Neurosci. XXXX, XXX, XXX−XXX

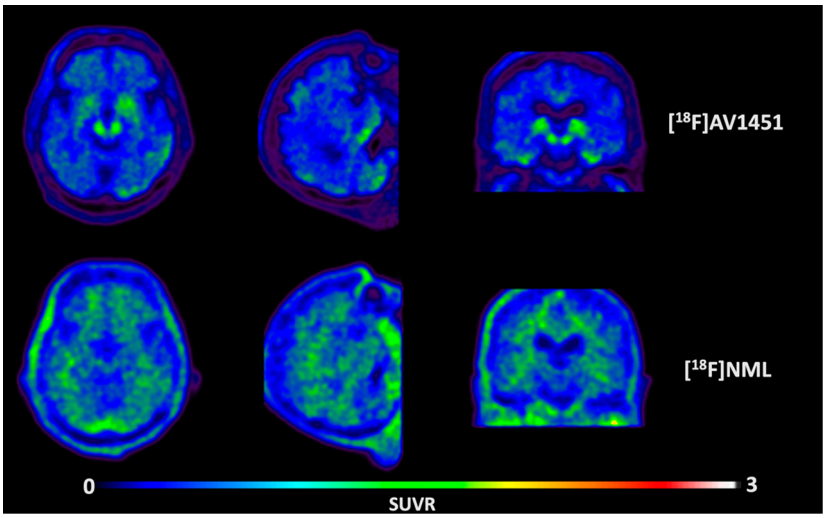

Figure 4. Transversal, sagittal, and coronal view of averaged PET images of [^{18}F]AV1451 (upper row) and [^{18}F]NML (lower row) uptake in a PSP patient 80−100 and 60−90 min p.i., respectively.

brain retention in MCI/AD and PSP patients was low, and there was no evidence of specific binding to tau *in vivo*. As such, we conclude that further development of [^{18}F]NML as a tau PET imaging agent is not warranted at this time.

METHODS

PositronMed. *General Information.* The study at PositronMed was approved by the institutional and regional ethic committee boards (Comité de Ética Científico, Servicio de Salud Metropolitano Oriente, permit 20160405 and 20161025). Inclusion criteria for all participants were written informed consent and use of anticontraceptives for at least six months after last imaging visit in case of possible pregnancy. Healthy volunteers had to be age 50−70 years, without having clinical signs of any neurological disorder as evaluated by standard neurological exams. Inclusion criteria for AD patients were age 50−90 years having a clinical diagnose of AD based on NINCDS/ADRDA and DSM-IV criteria and the ability to follow the study procedures.

Radiotracers. Production of [^{18}F]NML was carried out using a cassette based module (IBA Synthera) using a minor modification of the conditions developed by Riss et al.[29] The [^{18}F]fluoride was produced with an IBA Cyclone 18/9 cyclotron by irradiation of 2.0 mL of [^{18}O]H_2O at 40−45 μA. [^{18}F]NML was synthesized using a Synthera V2 synthesis module and Synthera HPLC (Ion Bean Applications, Louvain-La-Neuve, Belgium) using a Synthera integrated fluidic processor (IFP) cassette purchased from ABX (Radeberg, Germany). The [^{18}F]fluoride from 2.0 mL of irradiated ^{18}O-water was trapped on a QMA-light Sep-Pak cartridge (Waters), eluted into the reaction vessel using a solution of aqueous K_2CO_3 (4.6 mg in 0.3 mL of water) and crypt-222 (22 mg in 0.3 mL of acetonitrile), and dried by evaporation. A solution of precursor **1** (2.5 mg) in anhydrous DMSO (650 μL) and isopropanol (36 μL) was added, and the solution was heated at 90 °C for 3 min. After cooling to 50 °C, the reaction mixture was diluted with mobile phase (1.5 mL) and purified by semipreparative HPLC (column, Phenomenex Luna PFP(2) 250 × 10 mm^2; mobile phase, 65% water in 35% acetonitrile (v/v); flow rate, 3.5 mL/min). The fraction corresponding to [^{18}F]NML (typically eluting around 26 min) was collected and transferred into a dilution flask containing sterile water (50 mL). The product was reformulated from the resulting solution by trapping on a Strata-X 33 mg cartridge (Phenomenex), rinsing with sterile water (3 mL), elution into a second collection vial with ethanol for injection (1.0 mL), and dilution with 0.9% sodium chloride for injection (9.0 mL). The final isotonic formulation (10 mL) was passed through a 0.22 μM Millex-GV sterile filter (Millipore, Billerica, MA) into a sterile vial to provide [^{18}F]NML. Typically 2.3 ± 1.4 GBq (2.1% ± 1.4% non-decay-corrected RCY) of [^{18}F]NML was obtained from 111.6 ± 25.8 GBq of [^{18}F]fluoride, n = 5 (see Supporting Information for details).

[^{18}F]AV1451 was prepared as previously described,[37] and [^{18}F]-florbetaben was obtained from Positronpharma SA.

QC Testing. Quality control testing was conducted according to the standard procedures outlined in the US Pharmacopeia (see Supporting Information for details and Table 1 for full quality control test results). The final formulation of [^{18}F]NML had a pH of 5.0, and radiochemical purity was >97%.

PET Imaging. [^{18}F]NML PET/CT. At PositronMed, all subjects were scanned with a Siemens mCT Flow PET scanner (Siemens, Erlangen, Germany). Daily QC of the PET scanner was performed and passed at each imaging visit. Activity calibration of the scanner was performed by phantom measurements according to standard procedures. The mean ± SD of the administered mass of [^{18}F/^{19}F]NML was 1.06 ± 0.61 μg (range, 0.16−1.61 μg), and the mean administered activity was 296.9 ± 55.9 MBq (range, 199−339 MBq). There were no adverse or clinically detectable pharmacologic effects in any of the 5 subjects, and no significant changes in vital signs were observed. Subjects were placed supine with their head secured with fixation straps. Attenuation correction CT was performed prior to PET acquisition. The CT parameters were 120 kV with dose modulation (CARE Dose4D), reconstruction thickness 3 mm (configuration 20 × 0.6 mm^2), pitch of 0.55, and rotation cycle of 1 s. Following CT acquisition, subjects received a single intravenous bolus of [^{18}F]NML within approximately 6 s while dynamic PET acquisition was simultaneously started. The emission scan was acquired in LIST-Mode for 90 min and reconstructed with the following parameters and corrections: time frames 10 × 6 s, 6 × 20 s, 7 × 60 s, 5 × 120 s, 14 × 300 s; Gaussian filter, fwhm 2.0, 5 iterations, 21 subsets, matrix 256 × 256, attenuation and scatter correction.

[^{18}F]AV1451 PET/CT. As described by Shcherbinin and colleagues,[34] subjects received a single intravenous bolus of 391 ± 13 MBq of [^{18}F]AV1451 within approximately 6 s and were allowed to rest for 70 min before being placed supine with their head secured with fixation straps. Attenuation correction CT was performed prior to PET acquisition with the following parameters: 120 kV with dose modulation (CARE Dose4D), reconstruction thickness 3 mm (configuration 20 × 0.6 mm^2), pitch of 0.55, and rotation cycle of 1 s. PET emission scans were acquired in LIST-mode from 80 to 100 min postinjection and reconstructed with the following parameters and corrections: Time frames 4 × 300 s; Gaussian filter, fwhm 2.0, 5 iterations, 21 subsets, matrix 256 × 256, attenuation and scatter correction.

https://dx.doi.org/10.1021/acschemneuro.9b00639
ACS Chem. Neurosci. XXXX, XXX, XXX−XXX

MRI Scans. Three of five subjects were scanned in a 1.5 T magnetic resonance imaging (MRI) scanner from Gyroscan Intera, Phillips Medical System, Best, the Netherlands. Three-dimensional, T1-weighted MR images (isotropic 1 × 1 × 1 mm^3 resolution) were acquired using the following parameters: T1 protocol; repetition time = 7.3 ms; echo delay time 3.3 ms; inversion time = 815 ms; flip angle = 8°. Images were used for co-registration and normalization of corresponding PET images.

University of Michigan. *General Information.* The experimental procedures were approved by the University of Michigan Institutional Review Board (HUM00124161: Evaluation of Tau Imaging Radiotracers) and the Radioactive Drug Research Committee (RDRC) overseeing the use of radionuclides in humans. All subjects gave written informed consent before study participation. Subjects were screened within 30 d before PET, including recording of demographic information, clinical history, concomitant medications, physical and neurologic examination, and neuropsychologic testing.

Radiotracers. Production of [^{18}F]NML was carried out in a GE tracerlab FX_{FN} synthesis module in a manner consistent with the original report.[25] A GE PETtrace cyclotron was utilized to prepare [^{18}F]fluoride by irradiation of 1.5 mL of [^{18}O]H_2O at 40 μA. [^{18}F]NML was synthesized using a GE TRACERLab FX_{FN} synthesis module. The [^{18}F]fluoride (approximately 66.6 GBq) was trapped on a QMA-light Sep-Pak cartridge (Waters) that had been preconditioned with $KHCO_3$ solution (0.5 M). [^{18}F]Fluoride was eluted with a solution of K_2CO_3 (3.5 mg) in water (0.5 mL). A solution of cryptand-222 (15 mg) in acetonitrile (1 mL) was then added to the reactor, and the [^{18}F]fluoride was azeotropically dried. A solution of precursor **1** (3.5 mg) in anhydrous DMSO (950 μL) and satd. NH_4Cl solution (5 μL) was added, and the solution was heated at 90 °C for 3 min. After cooling to 50 °C, the reaction mixture was diluted with HPLC mobile phase (3 mL) and purified by semipreparative HPLC (column, Phenomenex Luna PFP(2) 250 × 10 mm^2; mobile phase, 70% water in 30% acetonitrile (v/v); flow rate, 4.0 mL/min). The fraction corresponding to [^{18}F]NML (typically eluting around 35 min) was collected and transferred into a dilution flask containing sterile water (50 mL). The product was reformulated from the resulting solution by trapping on a 1 cm^3 C18 cartridge (Waters), rinsing with sterile water (10 mL), eluting into a second collection vial with ethanol for injection (0.5 mL), and dilution with 0.9% sodium chloride for injection (9.5 mL). The final isotonic formulation (10 mL) was passed through a 0.22 μM Millex-GV sterile filter (Millipore, Billerica, MA) into a sterile vial to provide [^{18}F]NML. Typically 3.9 ± 1.4 GBq (5.9% ± 2.0% non-decay-corrected RCY) of [^{18}F]NML was obtained from approximately 66.6 GBq of [^{18}F]fluoride (estimated from known cyclotron production history), n = 10 (4 validation runs and 6 clinical production batches; see Supporting Information for full details).

[^{18}F]AV1451 was prepared as previously described,[37] and [^{18}F]-florbetapir was obtained from Avid Radiopharmaceuticals.

QC Testing. Quality control testing was conducted according to the standard procedures outlined in the US Pharmacopeia (see Supporting Information for details and Table 1 for full quality control test results). The final formulation of [^{18}F]NML had a pH of 5.0, and radiochemical purity was 100%.

QC testing of [^{18}F]AV1451 was conducted as previously described.[37]

PET Imaging. [^{18}F]NML and [^{18}F]AV1451 PET/CT. At the University of Michigan, the mean ± SD of the administered mass of [^{18}F/^{19}F]NML was 2.80 ± 2.73 μg (range, 1.05−8.27 μg) and the mean administered activity was 395.2 ± 8.0 MBq (range, 384−403 MBq). There were no adverse or clinically detectable pharmacologic effects in any of the 6 subjects scanned at UM, and no significant changes in vital signs were observed. PET imaging sessions were conducted for both [^{18}F]NML and [^{18}F]AV1451 on separate 1/2-day study visits using a Siemens BioGraph TruePoint PET-CT (model 1094). Subjects were scanned with eyes and ears not occluded in a dimly lit scanning environment. The procedures employed were identical for each PET imaging agent. Subjects were positioned on the PET scanner table, lying on their back. They were asked to lie quietly, to stay awake, and to keep their eyes open during the PET scans. An IV was placed in one arm, and a low-dose X-ray CT scan of the head was performed for attenuation correction of emission PET images. The PET tracer (10 mCi of either [^{18}F]NML or [^{18}F]AV1451 on separate PET imaging visits) was injected as an IV bolus. First, dynamic PET imaging began immediately and was collected for 60 min: 4 × 30 s frames; 3 × 1 min frames, 2 × 2.5 min frames; 6 × 5 min; 2 × 10 min. After a several minute break, additional brain images were made from 75−105 min: 3 × 10 min. Subjects were then removed from the PET scanner, and the IV tube was removed, ending the visit.

Other Method Considerations. *Scanner Considerations.* PET/CT scanners at each site were calibrated. However, we did not perform a cross-calibration of the two scanners used at the different sites. Reflecting this, SUVs may differ slightly between sites and were thus not compared directly. The lack of cross-calibration should not affect comparisons of SUVR values.

The different frame settings at each site results from site specific PET imaging and reconstruction protocols. Since there is no specific binding of [^{18}F]NML to tau, and we did not compare subjects between sites, these protocols were not standardized.

Image Analysis. Image postacquistion processing was carried out using the Pmod quantification software, v3.4 (PMOD Technologies Ltd., Zurich, Switzerland). PET images were corrected for motion and, if available, co-registered to individual T1 weighted MRI scans and normalized to Montreal Neurological Institute (MNI) space using the PNeuro tool. Standard VOI maps were outlined from the available brain atlas in MNI space[38] for cortical gray matter regions (frontal cortex, parietal cortex, temporal cortex, occipital cortex, neocortex, putamen, hippocampus, and different subregions of temporal cortex) and cerebellar cortex as reference region. Time−activity curves (TACs) and average standard uptake values (SUVs) at different time points were calculated for all brain regions. Specific uptake value ratios (SUVRs) were calculated as SUVR = (SUV region/SUV cerebellum) for all regions, and brain uptake was calculated in percent injected dose (% i.D.) in the whole brain at different time points.

■ ASSOCIATED CONTENT

Supporting Information

The Supporting Information is available free of charge at https://pubs.acs.org/doi/10.1021/acschemneuro.9b00639.

Chemistry investigations, biodistribution studies, human dosimetry estimates, radiosynthesis data, and quality control testing of [^{18}F]NML (PDF)

■ AUTHOR INFORMATION

Corresponding Authors

Vasko Kramer − *Center for Nuclear Medicine & PET/CT Positronmed, Providencia, Chile, and Positronpharma SA, Providencia, Chile;* orcid.org/0000-0002-5285-6447; Email: vkramer@positronpharma.cl

Allen F. Brooks − *University of Michigan, Ann Arbor, Michigan;* orcid.org/0000-0003-3773-3024; Email: afb@umich.edu

Peter J. H. Scott − *University of Michigan, Ann Arbor, Michigan;* orcid.org/0000-0002-6505-0450; Email: pjhscott@umich.edu

Patrick J. Riss − *Universitetet i Oslo, Oslo, Norway, Oslo Universitets Sykehus HF−Rikshospitalet, Oslo, Norway, and Norsk Medisinsk Syklotronsenter AS, Gaustad, Oslo, Norway;* orcid.org/0000-0002-3887-7065; Email: patrick.riss@kjemi.uio.no

https://dx.doi.org/10.1021/acschemneuro.9b00639
ACS Chem. Neurosci. XXXX, XXX, XXX−XXX

Other Authors

Arlette Haeger − *Center for Nuclear Medicine & PET/CT Positronmed, Providencia, Chile*

Rodrigo Kuljis − *Center for Nuclear Medicine & PET/CT Positronmed, Providencia, Chile*

Waqas Rafique − *Universitetet i Oslo, Oslo, Norway*

Robert A. Koeppe − *University of Michigan, Ann Arbor, Michigan*

David M. Raffel − *University of Michigan, Ann Arbor, Michigan;* orcid.org/0000-0002-7188-9463

Kirk A. Frey − *University of Michigan, Ann Arbor, Michigan*

Horacio Amaral − *Center for Nuclear Medicine & PET/CT Positronmed, Providencia, Chile, and Positronpharma SA, Providencia, Chile*

Complete contact information is available at: https://pubs.acs.org/10.1021/acschemneuro.9b00639

Author Contributions

[▽]V.K. and A.F.B. contributed equally. All authors contributed to writing this article.

Funding

Financial support for this work from the Alzheimer's Association (NIRP-14-305669 to P.J.H.S.), University of Michigan Department of Radiology (startup funds to P.J.H.S.), the National Institutes of Health's National Center for Advancing Translational Sciences (NCATS) Clinical and Translational Science Awards (CTSA) Program for pilot funds provided through the Michigan Institute for Clinical & Health Research (MICHR) (UL1TR002240 to A.F.B.), a grant from InnovaChile (CORFO, project 14IEAT-28666), and the REALOMICS SFI, Universitetet i Oslo (P.J.R.) is gratefully acknowledged.

Notes

The authors declare no competing financial interest.

■ ACKNOWLEDGMENTS

We thank all of the subjects and their families for participation in the study. In addition, we thank Phillip Sherman, Jenelle Stauff, and Janna Arteaga for conducting rodent biodistribution studies, and Bradford Henderson for conducting quality control testing on [^{18}F]NML doses at the University of Michigan.

■ ABBREVIATIONS USED

AD, Alzheimer's disease; MCI, mild cognitive impairment; NFT, neurofibrillary tangle; NML, *N*-methyl lansoprazole; PET, positron emission tomography

■ REFERENCES

(1) Lowe, V. J., Wiste, H. J., Senjem, M. L., Weigand, S. D., Therneau, T. M., Boeve, B. F., Josephs, K. A., Fang, P., Pandey, M. K., Murray, M. E., Kantarci, K., Jones, D. T., Vemuri, P., Graff-Radford, J., Schwarz, C. G., Machulda, M. M., Mielke, M. M., Roberts, R. O., Knopman, D. S., Petersen, R. C., and Jack, C. R., Jr (2018) Widespread Brain Tau and its Association with Ageing, Braak Stage and Alzheimer's Dementia. *Brain 141*, 271−287.

(2) Giacobini, E., and Gold, G. (2013) Alzheimer disease therapy—moving from amyloid-β to tau. *Nat. Rev. Neurol. 9*, 677.

(3) Villemagne, V. L., Fodero-Tavoletti, M. T., Masters, C. L., and Rowe, C. C. (2015) Tau imaging: early progress and future directions. *Lancet Neurol. 14*, 114−124.

(4) Kolb, H. C., and Andrés, J. I. (2017) Tau positron emission tomography imaging. *Cold Spring Harbor Perspect. Biol. 9*, No. a023721.

(5) Saint-Aubert, L., Lemoine, L., Chiotis, K., Leuzy, A., Rodriguez-Vieitez, E., and Nordberg, A. (2017) Tau PET imaging: present and future directions. *Mol. Neurodegener. 12*, 19.

(6) Okamura, N., Harada, R., Ishiki, A., Kikuchi, A., Nakamura, T., and Kudo, Y. (2018) The Development and Validation of Tau PET Tracers: Current Status and Future Directions. *Clin. Transl. Imaging 6*, 305−316.

(7) Villemagne, V. L., Doré, V., Burnham, S. C., Masters, C. L., and Rowe, C. C. (2018) Imaging tau and amyloid-β proteinopathies in Alzheimer disease and other conditions. *Nat. Rev. Neurol. 14*, 225−236.

(8) Wang, Y. T., and Edison, P. (2019) Tau imaging in neurodegenerative diseases using positron emission tomography. *Curr. Neurol. Neurosci. Rep. 19*, 45.

(9) Brosch, J. R., Farlow, M. R., Risacher, S. L., and Apostolova, L. G. (2017) Tau Imaging in Alzheimer's Disease Diagnosis and Clinical Trials. *Neurotherapeutics 14*, 62−68.

(10) Harada, R., Okamura, N., Furumoto, S., Furukawa, K., Ishiki, A., Tomita, N., Tago, T., Hiraoka, K., Watanuki, S., Shidahara, M., Miyake, M., Ishikawa, Y., Matsuda, R., Inami, A., Yoshikawa, T., Funaki, Y., Iwata, R., Tashiro, M., Yanai, K., Arai, H., and Kudo, Y. (2016) ^{18}F-THK5351: A Novel PET Radiotracer for Imaging Neurofibrillary Pathology in Alzheimer Disease. *J. Nucl. Med. 57*, 208−14.

(11) Xia, C.-F., Arteaga, J., Chen, G., Gangadharmath, U., Gomez, L. F., Kasi, D., Lam, C., Liang, Q., Liu, C., Mocharla, V. P., Mu, F., Sinha, A., Su, H., Szardenings, A. K., Walsh, J. C., Wang, E., Yu, C., Zhang, W., Zhao, T., and Kolb, H. C. (2013) [^{18}F]T807, a novel tau positron emission tomography imaging agent for Alzheimer's disease. *Alzheimer's Dementia 9*, 666−676.

(12) Ng, K. P., Pascoal, T. A., Mathotaarachchi, S., Therriault, J., Kang, M. S., Shin, M., Guiot, M.-C., Guo, Q., Harada, R., Comley, R. A., Massarweh, G., Soucy, J.-P., Okamura, N., Gauthier, S., and Rosa-Neto, P. (2017) Monoamine oxidase B inhibitor, selegiline, reduces 18F- THK5351 uptake in the human brain. *Alzheimer's Res. Ther. 9*, 25.

(13) Drake, L. R., Pham, J. M., Desmond, T. J., Mossine, A. V., Lee, S. J., Kilbourn, M. R., Koeppe, R. A., Brooks, A. F., and Scott, P. J. H. (2019) Identification of AV-1451 as a Weak, Nonselective Inhibitor of Monoamine Oxidase. *ACS Chem. Neurosci. 10*, 3839−3846.

(14) Lemoine, L., Leuzy, A., Chiotis, K., Rodriguez-Vieitez, E., and Nordberg, A. (2018) Tau positron emission tomography imaging in tauopathies: The added hurdle of off-target binding. *Alzheimer's Dement 10*, 232−236.

(15) Kimura, Y., Ichise, M., Ito, H., Shimada, H., Ikoma, Y., Seki, C., Takano, H., Kitamura, S., Shinotoh, H., Kawamura, K., Zhang, M. R., Sahara, N., Suhara, T., and Higuchi, M. (2015) PET Quantification of Tau Pathology in Human Brain with ^{11}C-PBB3. *J. Nucl. Med. 56*, 1359−65.

(16) Hostetler, E. D., Walji, A. M., Zeng, Z., Miller, P., Bennacef, I., Salinas, C., Connolly, B., Gantert, L., Haley, H., Holahan, M., Purcell, M., Riffel, K., Lohith, T. G., Coleman, P., Soriano, A., Ogawa, A., Xu, S., Zhang, X., Joshi, E., Della Rocca, J., Hesk, D., Schenk, D. J., and Evelhoch, J. L. (2016) Preclinical Characterization of ^{18}F-MK-6240, a Promising PET Tracer for In Vivo Quantification of Human Neurofibrillary Tangles. *J. Nucl. Med. 57*, 1599−1606.

(17) Pascoal, T. A., Shin, M., Kang, M. S., Chamoun, M., Chartrand, D., Mathotaarachchi, S., Bennacef, I., Therriault, J., Ng, K. P., Hopewell, R., Bouhachi, R., Hsiao, H. H., Benedet, A. L., Soucy, J. P., Massarweh, G., Gauthier, S., and Rosa-Neto, P. (2018) In vivo quantification of neurofibrillary tangles with [^{18}F]MK-6240. *Alzheimer's Res. Ther. 10*, 74.

(18) Kroth, H., Oden, F., Molette, J., Schieferstein, H., Capotosti, F., Mueller, A., Berndt, M., Schmitt-Willich, H., Darmency, V., Gabellieri, E., Boudou, C., Juergens, T., Varisco, Y., Vokali, E., Hickman, D. T., Tamagnan, G., Pfeifer, A., Dinkelborg, L., Muhs, A., and Stephens, A.

(2019) Discovery and preclinical characterization of [18F]PI-2620, a next-generation tau PET tracer for the assessment of tau pathology in Alzheimer's disease and other tauopathies. *Eur. J. Nucl. Med. Mol. Imaging 46*, 2178−2189.

(19) Sanabria Bohórquez, S., Marik, J., Ogasawara, A., Tinianow, J. N., Gill, H. S., Barret, O., Tamagnan, G., Alagille, D., Ayalon, G., Manser, P., Bengtsson, T., Ward, M., Williams, S. P., Kerchner, G. A., Seibyl, J. P., Marek, K., and Weimer, R. M. (2019) [^{18}F]GTP1 (Genentech Tau Probe 1), a radioligand for detecting neurofibrillary tangle tau pathology in Alzheimer's disease. *Eur. J. Nucl. Med. Mol. Imaging 46*, 2077−2089.

(20) Kuwabara, H., Comley, R. A., Borroni, E., Honer, M., Kitmiller, K., Roberts, J., Gapasin, L., Mathur, A., Klein, G., and Wong, D. F. (2018) Evaluation of 18F-RO-948 PET for Quantitative Assessment of Tau Accumulation in the Human Brain. *J. Nucl. Med. 59*, 1877−1884.

(21) Shimada, H., Kitamura, S., Ono, M., Kimura, Y., Ichise, M., Takahata, K., Moriguchi, S., Kubota, M., Ishii, T., Takado, Y., Seki, C., Hirano, S., Shinotoh, H., Sahara, N., Tempest, P., Tamagnan, G., Seibyl, J., Barret, O., Alagille, D., Zhang, M.-R., Kuwabara, S., Jang, M.-K., Marek, K., Suhara, T., and Higuchi, M. (2017) First-in-human PET study with ^{18}F-AM-PBB3 and ^{18}F-PM-PBB3. *Alzheimer's Dementia 13*, P146.

(22) Villemagne, V., Dore, V., Mulligan, R., Lamb, F., Bourgeat, P., Salvado, O., Masters, C., and Rowe, C. (2018) Evaluation of ^{18}F-PI-2620, a second-generation selective tau tracer for the assessment of Alzheimer's and non-Alzheimer's tauopathies. *Alzheimer's Dementia 14*, P1021.

(23) Leuzy, A., Chiotis, C., Lemoine, L., Gillberg, P.-G., Almkvist, O., Rodriguez-Vieitez, E., and Nordberg, A. (2019) Tau PET Imaging in Neurodegenerative Tauopathies—Still a Challenge. *Mol. Psychiatry 24*, 1112−1134.

(24) Rojo, L. E., Alzate-Morales, J., Davies, P., Maccioni, R. B., and Saavedra, I. N. (2010) Selective Interaction of Lansoprazole and Astemizole with Tau Polymers: Potential New Clinical Use in Diagnosis of Alzheimer's Disease. *J. Alzheimer's Dis. 19*, 573−589.

(25) Fawaz, M. V., Brooks, A. F., Rodnick, M. E., Carpenter, G. M., Shao, X., Desmond, T. J., Sherman, P., Quesada, C. A., Hockley, B. G., Kilbourn, M. R., Albin, R. L., Frey, K. A., and Scott, P. J. H. (2014) High Affinity Radiopharmaceuticals Based Upon Lansoprazole for PET Imaging of Aggregated Tau in Alzheimer's Disease and Progressive Supranuclear Palsy: Synthesis, Preclinical Evaluation, and Lead Selection. *ACS Chem. Neurosci. 5*, 718−730.

(26) Shao, X., Carpenter, G. M., Desmond, T. J., Sherman, P., Quesada, C. A., Fawaz, M. V., Brooks, A. F., Kilbourn, M. R., Albin, R. L., Frey, K. A., and Scott, P. J. H. (2012) Evaluation of [^{11}C]N-Methyl Lansoprazole as a Radiopharmaceutical for PET Imaging of Tau Neurofibrillary Tangles. *ACS Med. Chem. Lett. 3*, 936−941.

(27) Rafique, W., Kramer, V., Pardo, T., Smits, R., Spilhaug, M. M., Hoepping, A., Savio, E., Engler, H., Kuljs, R., Amaral, H., and Riss, P. J. (2018) Image-Guided Development of Heterocyclic Sulfoxides as Ligands for Tau Neurofibrillary Tangles: From First-in-Man to Second-Generation Ligands. *ACS Omega 3*, 7567−7579.

(28) Brooks, A., Burris, S., and Scott, P. (2017) Binding of [^{18}F]N-Methyl Lansoprazole to Tau Aggregates in Post-Mortem Brain Sections from Alzheimer's Disease and Progressive Supranuclear Palsy Patients. *J. Nucl. Med. 58* (Suppl. 1), 553.

(29) Riss, P. J., Ferrari, V., Brichard, L., Burke, P., Smith, R., and Aigbirhio, F. I. (2012) Direct, nucleophilic radiosynthesis of [^{18}F]trifluoroalkyl tosylates: improved labelling procedures. *Org. Biomol. Chem. 10*, 6980−6986.

(30) Brooks, A. F., Topczewski, J. T., Ichiishi, N., Sanford, M. S., and Scott, P. J. H. (2014) Late-stage [^{18}F]fluorination: new solutions to old problems. *Chem. Sci. 5*, 4545−4553.

(31) Stabin, M. G., Sparks, R. B., and Crowe, E. (2005) OLINDA/EXM: The Second-Generation Personal Computer Software for Internal Dose Assessment in Nuclear Medicine. *J. Nucl. Med. 46*, 1023−1027.

(32) Okamura, N., Furumoto, S., Fodero-Tavoletti, M. T., Mulligan, R. S., Harada, R., Yates, P., Pejoska, S., Kudo, Y., Masters, C. L., Yanai, K., Rowe, C. C., and Villemagne, V. L. (2014) Non-invasive assessment of Alzheimer's disease neurofibrillary pathology using ^{18}F-THK5105 PET. *Brain 137*, 1762−1771.

(33) Ossenkoppele, R., Schonhaut, D. R., Schöll, M., Lockhart, S. N., Ayakta, N., Baker, S. L., O'Neil, J. P., Janabi, M., Lazaris, A., Cantwell, A., Vogel, J., Santos, M., Miller, Z. A., Bettcher, B. M., Vossel, K. A., Kramer, J. H., Gorno-Tempini, M. L., Miller, B. L., Jagust, W. J., and Rabinovici, G. D. (2016) Tau PET patterns mirror clinical and neuroanatomical variability in Alzheimer's disease. *Brain 139*, 1551−67.

(34) Shcherbinin, S., Schwarz, A. J., Joshi, A., Navitsky, M., Flitter, M., Shankle, W. R., Devous, M. D., Sr., and Mintun, M. A. (2016) Kinetics of the Tau PET Tracer ^{18}F-AV-1451 (T807) in Subjects with Normal Cognitive Function, Mild Cognitive Impairment, and Alzheimer Disease. *J. Nucl. Med. 57*, 1535−1542.

(35) Whitwell, J. L., Lowe, V. J., Tosakulwong, N., Weigand, S. D., Senjem, M. L., Schwarz, C., Spychalla, A. J., Petersen, R. C., Jack, C. R., Jr, and Josephs, K. A. (2017) [^{18}F]AV-1451 tau-PET in progressive supranuclear palsy. *Mov. Disord. 32*, 124−133.

(36) Vermeiren, C., Motte, P., Viot, D., Mairet-Coello, G., Courade, J.-P., Citron, M., Mercier, J., Hannestad, J., and Gillard, M. (2018) The tau positron-emission tomography tracer AV-1451 binds with similar affinities to tau fibrils and monoamine oxidases. *Mov. Disord. 33*, 273−281.

(37) Mossine, A. V., Brooks, A. F., Henderson, B. D., Hockley, B. G., Frey, K. A., and Scott, P. J. H. (2017) An updated radiosynthesis of [^{18}F]AV1451 for tau PET imaging. *EJNMMI Radiopharm. Chem. 2*, 7.

(38) Hammers, A., Allom, R., Koepp, M. J., Free, S. L., Myers, R., Lemieux, L., Mitchell, T. N., Brooks, D. J., and Duncan, J. S. (2003) Three-dimensional maximum probability atlas of the human brain, with particular reference to the temporal lobe. *Hum Brain Mapp 19*, 224−247.

https://dx.doi.org/10.1021/acschemneuro.9b00639
ACS Chem. Neurosci. XXXX, XXX, XXX−XXX